

SYSTEM IDENTIFICATION USING FLIGHT TEST DATA AND MACHINE LEARNING

Roger Larsson[1,2]

[1]Saab Aeronautics
[2]Linköping University

Abstract

The usability of a flight mechanical simulation model relies heavily on the sub-models included. One of the more important ones is the aerodynamic model. In this paper, a method for estimating nonlinear aerodynamic properties, using flight test data in combination with a machine learning method based on neural networks, is investigated. The results are compared to using linear system estimation, which must be done at several set points to get nonlinear behavior. The application used here is a subscale radio-controlled demonstrator aircraft for which data from wind tunnel testing, CFD calculations and flight testing exist. The result shows that using Neural Network functions for system identification is possible. It can handle nonlinear system behavior. Since the method relies heavily on data available, as much data as possible should be used to cover the envelope of interest. Outside this envelope the model becomes unreliable.

Keywords: System identification, Subscale aircraft, Flight test, Machine Learning

1. Introduction

System identification for flight test evaluation helps build better flight mechanical models that can be used for flight control law design leading to better performance. A flight mechanical model in Simulink has been built for the work described in this paper. The structure of this model is given in Figure 1.

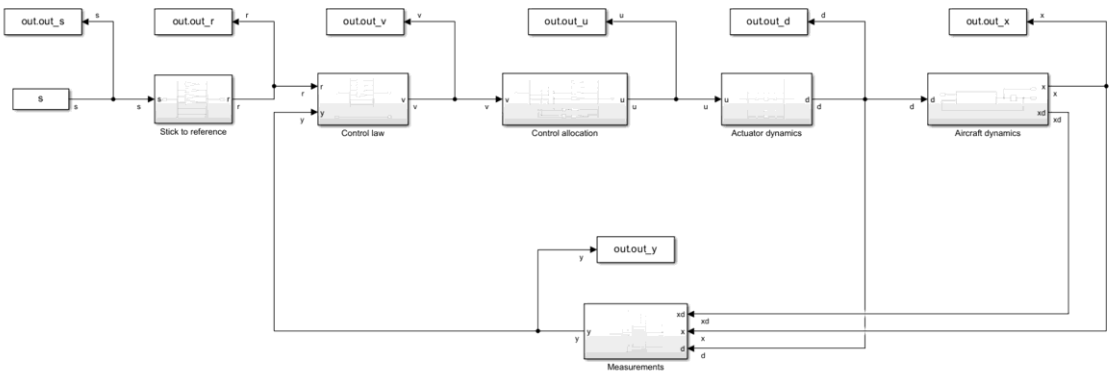


Figure 1 – Flight mechanical Simulink® model.

One of the more important sub-models is the one that describes aerodynamic properties. A subscale radio-controlled demonstrator aircraft called GFF [1] has been used as an application. This aircraft is shown in Figure 2. This aircraft has a 1.5 m span, weighs about 20 kg, and has a jet engine with a max thrust of 160 N. The use of subscale flight testing in design has been investigated in [2] and [3].



Figure 2 – Subscale radio-controlled demonstrator aircraft called GFF.

Definitions of the flight mechanical parameters used are shown in Figure 3. Note that a body-oriented system is used in this work with the origin in the aircraft center-of-gravity. The aerodynamic force coefficients are for the tangential (C_T), side (C_C) normal (C_N) force respectively. The moment coefficients are for the rolling moment (C_l), the pitching moment (C_m) and the yawing moment (C_n). These are functions of the velocity vector components including speed (V), angle-of-attack (α) and sideslip angle (β) and the angular velocities for roll (p), pitch (q) and yaw (r) as well as the control surface deflection for the left and right elevons (δ_{LE}, δ_{RE}) and the left and right canard (δ_{LC}, δ_{RC}). The elevator (δ_e), aileron (δ_a) and canard (δ_c) deflections are defined as shown in Figure 3.

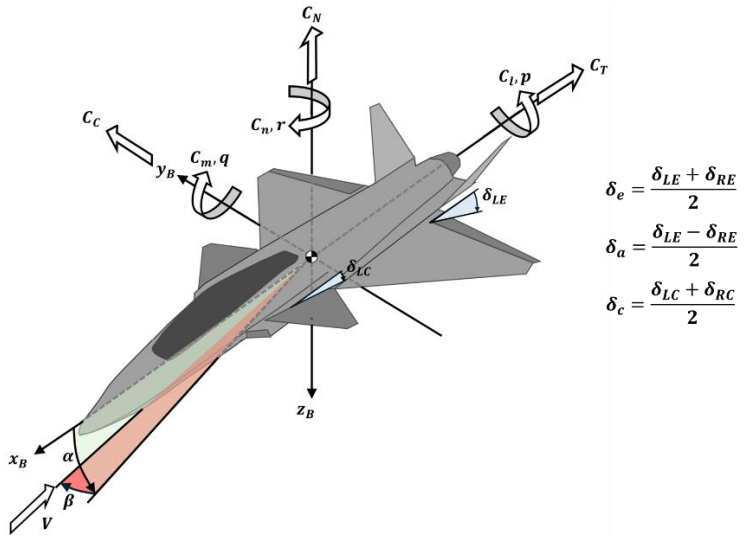


Figure 3 – definition of flight mechanical parameters for GFF.

Many CFD calculations have been performed to cover the envelope of the flight envelope for this aircraft. Some examples of these, showing the pressure coefficient (c_p), are given in Figure 4. A blue color means a low-pressure area and red means a high-pressure area. In Figures 5 and 6 the stability and main control model of the GFF are shown. Note that these are nonlinear functions. The damping effect due to the angular rotations, p, q and r is given as

$$C_{l_p} = \frac{\partial C_l}{\partial\left({}^{pb}/_{2V}\right)} = -0.23, \quad C_{m_q} = \frac{\partial C_m}{\partial\left({}^{qc}/_{2V}\right)} = -3.32 \text{ and } \quad C_{n_r} = \frac{\partial C_n}{\partial\left({}^{nb}/_{2V}\right)} = -0.62 \qquad (1)$$

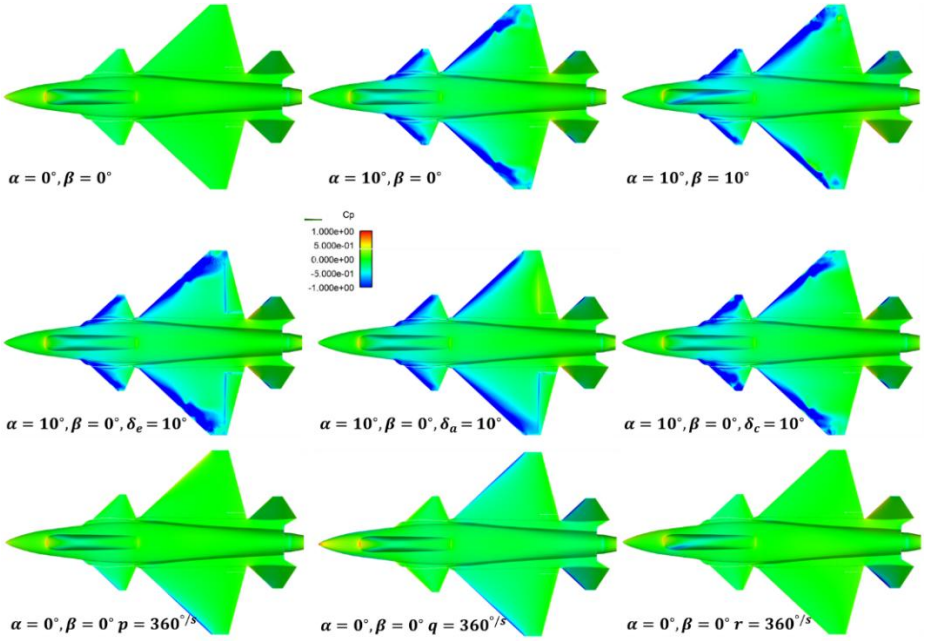


Figure 4 – Example of the pressure coefficient from CFD calculation of the GFF.

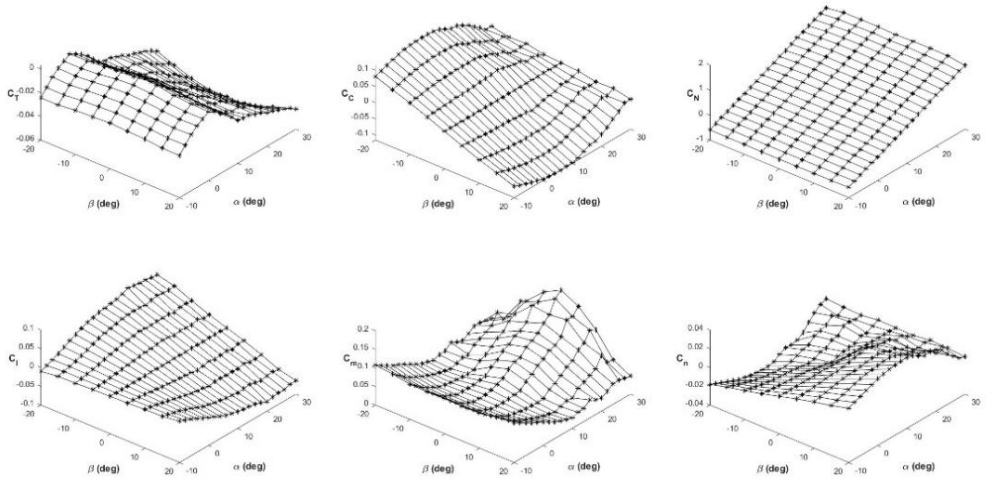


Figure 5 – Aerodynamic stability of the GFF.

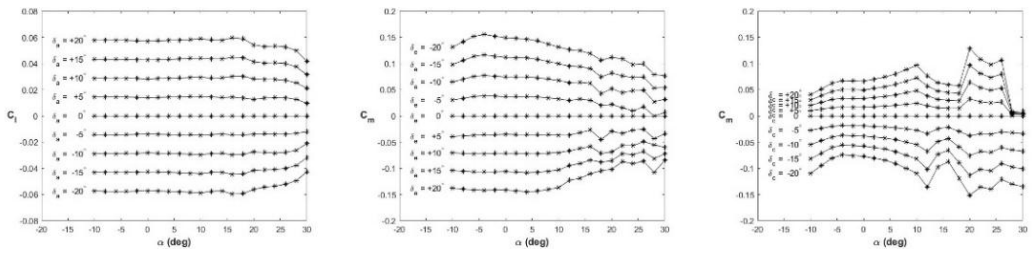


Figure 5 – Main aerodynamic control effectiveness of the GFF.

To be able to estimate an aerodynamic model, a system identification approach, based on raw flight test data has been used. Two methods have been used. The results are then compared, and conclusions are drawn on how well the methods work.

2. Methods

Two methods have been used for aerodynamic model estimation, one linear estimation method and one machine learning method using neural networks. These are described here.

2.1 Linear estimation

If the system is assumed to be linear, i.e., on the form A*x = b, a linear estimation, where the theory can be found in standard reference books [4]. For this the Matlab's built-in matrix left division function, also known as *backslash*, x = A\b can be used. This will be used in comparison with the Neural Network method investigated in this paper. The estimation using this method must be done at several set points to catch nonlinear behavior.

2.2 Machine Learning with Neural Networks

The main interest of this paper is to investigate the properties of the Matlab function for Neural Neatwork. An example of a neural network [5] is shown in Figure 6. This example has an input layer with four inputs, angle-of-attack (α), pitch angular velocity (q), elevator deflection angle (δ_e) and canard deflection angle (δ_c). There is also an output layer, which in this case has the normal force coefficient (C_N) as the output. Between the two layers are the hidden layers which consist of the neurons with the model parameters (θ) containing weights (w) and biases (b).

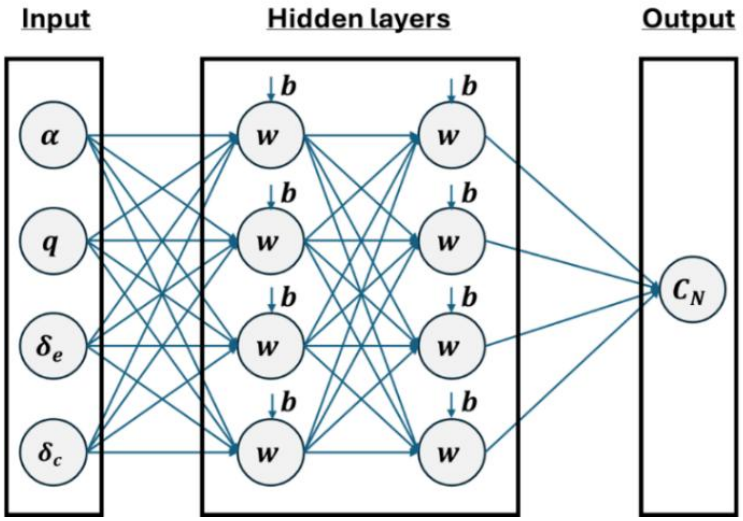


Figure 6 – An example neural network.

The output (a) from each neuron has the form

$$a = \sigma(z) \tag{3}$$

where σ is an activation function, which in this example is the sigmoid function

$$\sigma(z) = \frac{1}{1+e^{-z}} \tag{4}$$

and z is the weighted sum of each feature input to each neuron

$$z = \sum_{i=1}^{n} w_i x_i + b \tag{5}$$

2.3 Data

The flight test used comes from six flights with the GFF subscale demonstrator aircraft. Figure 7 shows the sensors implemented on the GFF. There is a data acquisition system onboard. Apart from that there are two inertial measurement units (IMU) that provide accelerations and angular velocities. Estimations of position, orientation and altitude are done by the IMUs together with GPS receivers, magnetometers, and air-pressure transducers. A custom-made nose-boom provides airspeed, angle-of-attack, and angle-of-sideslip. The system has also sensors for measuring control surface deflections. The signals are logged on board at an average sampling frequency of 100 Hz.

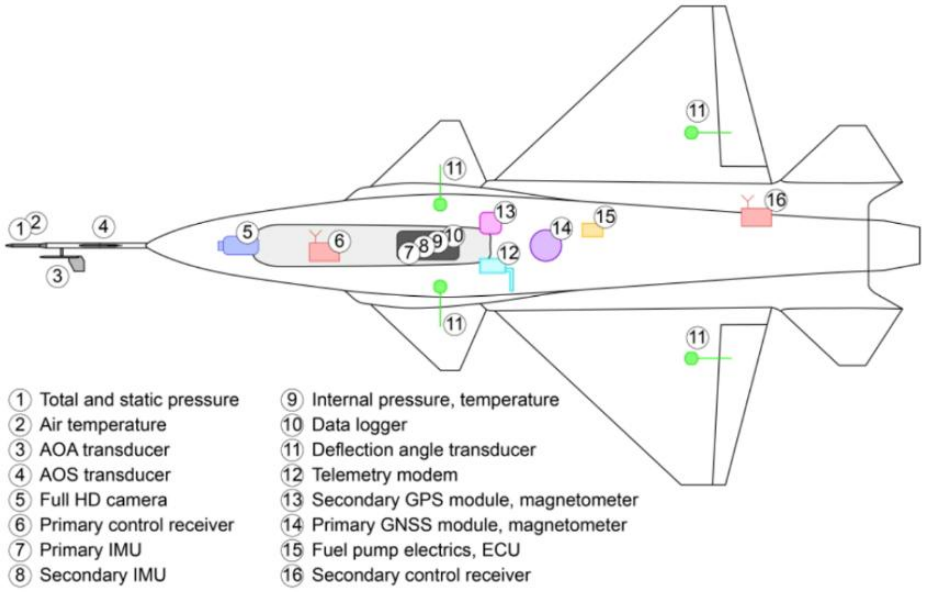


Figure 7 –GFF sensor equipment.

Figure 8 shows the sensor measurements of a 60 s interval from one of the flight tests. The first row shows the velocity vector $\boldsymbol{V} = [V \quad \alpha \quad \beta]$, the second row gives the Euler angles $\boldsymbol{\Phi} = [\phi \quad \theta \quad \psi]$, in row three the angular velocities $\boldsymbol{\omega_B} = [p \quad q \quad r]$ are given, the acceleration vector $\boldsymbol{a_B} = [a_x \quad a_y \quad a_z]$ is shown in row four, note that these are in the body system shown in Figure 3. The fifth row shows the control surface deflections $\boldsymbol{\delta} = [\delta_a \quad \delta_e \quad \delta_c]$, and finally in row six the altitude above ground h_g is shown together with the engine force F_{ENG} and engine angular velocity Ω_{ENG}. The aerodynamic forces and moments are calculated from the measurements using equation (5) – (10), which is given in [6]. Note that the engine force needs to be subtracted from the axial force coefficient $C_{X,s}$. The subscript *s* show that the calculations are done in the sensor position. The sensors are not located in the center-of-gravity. Their displacement is $\boldsymbol{\Delta} = [\Delta x \quad \Delta y \quad \Delta z]$, where $\Delta x = x_{CG} - x_s$, $\Delta y = y_{CG} - y_s$ and $\Delta z = z_{CG} - z_s$. To get the aerodynamic coefficients in the form specified in Figure 3, some of the forces needs to change signs and the moments need to be transformed from the sensor position to the center-of-gravity position. This change is given by equations (11) – (16) and the example sensor data given in Figure 8 which then results in the aerodynamic coefficient shown in Figure 9.

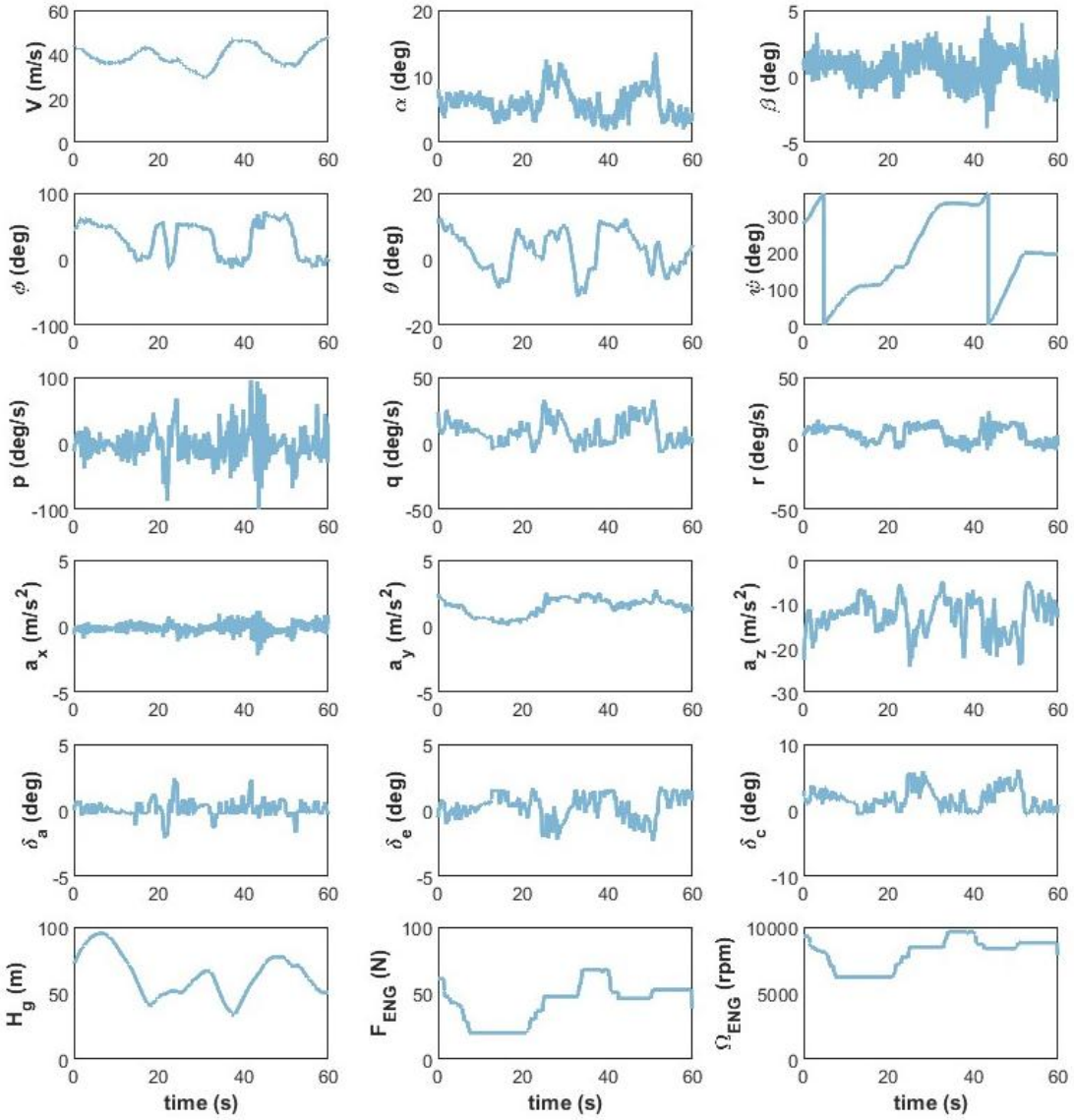


Figure 8 – Flight test data example for the GFF.

$$C_{X,s} = \frac{ma_x}{QS} - \frac{F_{ENG}}{QS} \tag{5}$$

$$C_{Y,s} = \frac{ma_y}{QS} \tag{6}$$

$$C_{Z,s} = \frac{ma_z}{QS} \tag{7}$$

$$C_{l,s} = \frac{I_{xx}}{QSb}\left[\dot{p} - \frac{I_{xz}}{I_{xx}}(\dot{r} + pq) + \frac{(I_{zz} - I_{yy})}{I_{xx}}qr\right] \tag{8}$$

$$C_{m,s} = \frac{I_{yy}}{QSc}\left[\dot{q} + \frac{I_{xz}}{I_{yy}}(p^2 - r^2) + \frac{(I_{xx} - I_{zz})}{I_{yy}}pr\right] \tag{9}$$

$$C_{n,s} = \frac{I_{zz}}{QSb}\left[\dot{r} - \frac{I_{xz}}{I_{zz}}(\dot{p} - qr) + \frac{(I_{yy} - I_{xx})}{I_{zz}}pq\right] \tag{10}$$

$$C_T = -C_x \tag{11}$$

$$C_C = C_Y \tag{12}$$

$$C_N = -C_Z \tag{13}$$

$$C_l = C_{l,s} + \Delta y\, C_N + \Delta z\, C_C \tag{14}$$

$$C_m = C_{m,s} + \Delta z\, C_T + \Delta x\, C_N \tag{15}$$

$$C_n = C_{n,s} + \Delta x\, C_C + \Delta y\, C_T \tag{16}$$

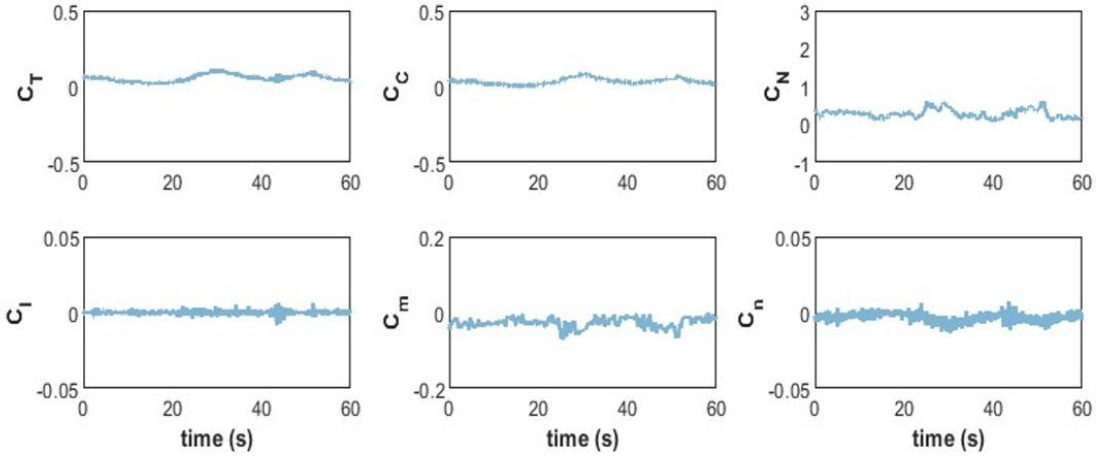


Figure 9 – Aerodynamic coefficients based on sensor data in Figure 8.

For the system identification, data from all six flight tests have been used. Figure 10 shows the flight test coverage compared to the CFD calculations and wind tunnel test performed. Most of the data is in the envelope, $0° \leq \alpha \leq 20°$ and $-5° \leq \beta \leq 5°$. There is a small amount of data below $\alpha = 0°$ and above $\alpha = 20°$, which will impact the estimations. Figure 10 also gives control surface deflections from all flight tests. The deflections are fairly limited in magnitude during the performed tests. However, the control surfaces can deflect more than this.

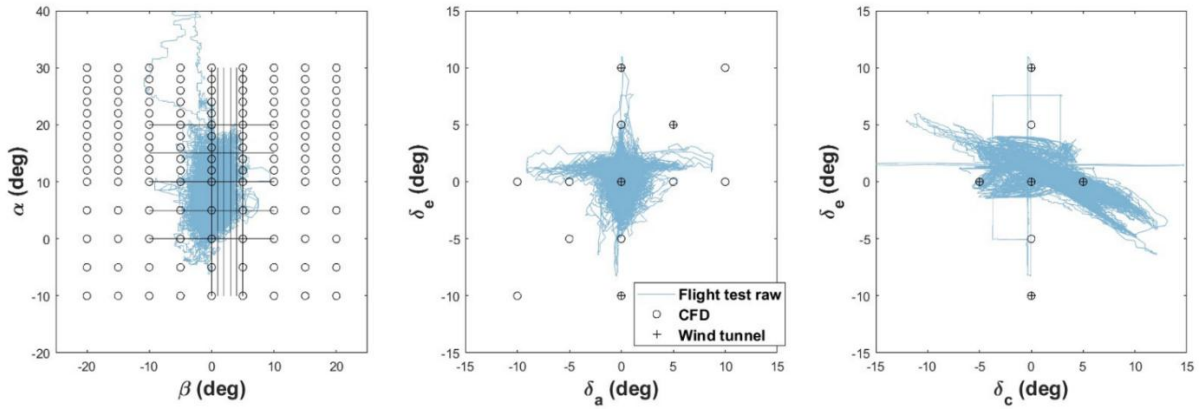


Figure 10 – Flight test data coverage compared to CFD and wind tunnel test.

The correlation between parameters used in the identification can affect the estimation of the model parameters. Figure 11 gives the correlation matrix for all the flight test data used. As can be seen, there are some correlations that can affect the results. The highest correlation is, $\rho(\delta_e, \delta_c) = -0.90$, between the elevator and canard deflections. This is not surprising since these control surfaces are coupled in the control allocation used in the radio control transmitter.

This is not the only correlation to look out for. The correlations, $\rho(V,\alpha) = -0.83$ and $\rho(q,\delta_c) = 0.86$ are also high.

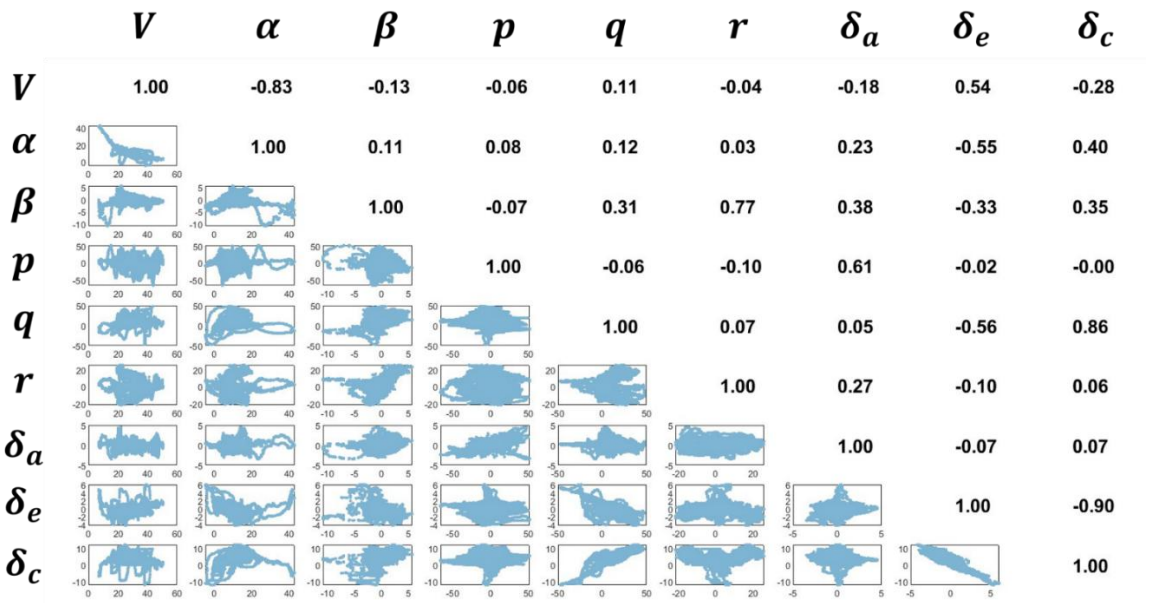


Figure 11 – Correlation matrix based on all flight test data used.

For the Linear estimation method data must be divided manually into parts to manage nonlinear data. In this paper, this linear estimation will be limited to the linear envelope, since not much data covering nonlinearities is available as can be seen in the CFD data in Figure 5 and the flight test coverage in Figure 10. It is possible to use a linear-in-parameter method for getting nonlinear model as in [7].

The Neural Network method will use all data available. When using the Neural Network function in Matlab®, the data will be automatically divided into three sets used for training, validation and testing the model. The amount of data going into the different parts is given by the user. The division 70% training, 15% validation and 15% testing data has been used in this paper.

3. Results

In Figure 12, the aerodynamic forces, and moments for the raw flight test data together with estimations based on this data as well as data from CFD calculations and wind tunnel tests are shown. For the longitudinal coefficients the data is plotted against angle-of-attack at zero sideslip angle and for the lateral/directional coefficients the data is plotted against sideslip angle at five degrees angle-of-attack, which is close to the trim angle. The Linear estimation method is shown in a red dashed line, and the Neural Network method is shown in a solid red line. The wind tunnel and CFD data given as black lines and black circles respectively. Also, the raw data from the flight test, which includes effects from the aileron, elevator and canard deflections, are shown in light blue to show where the flight test data is present.

The Neural Network method model accuracy for the training, validation and test data is given by Matlab®. Here, only the regression for the test data is shown in Figure 13. The accuracy is given by the coefficient of correlation value R, for which a value of 1 would be a perfect fit.

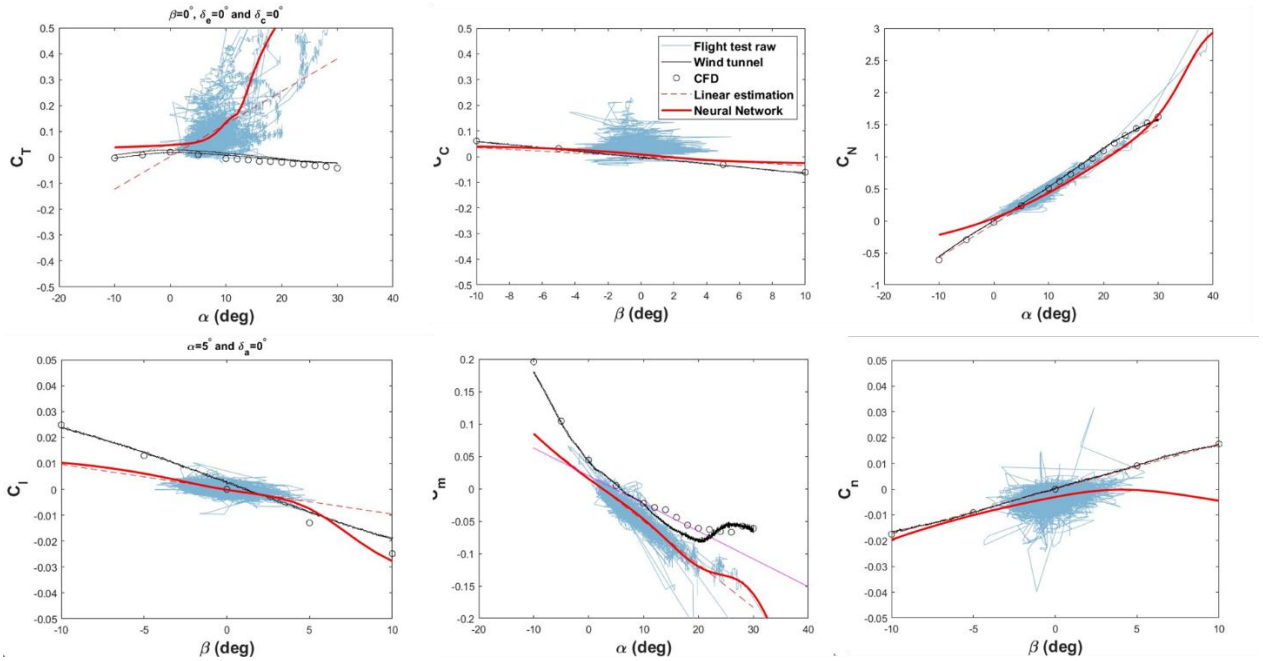


Figure 12 – Results for the aerodynamic coefficients.

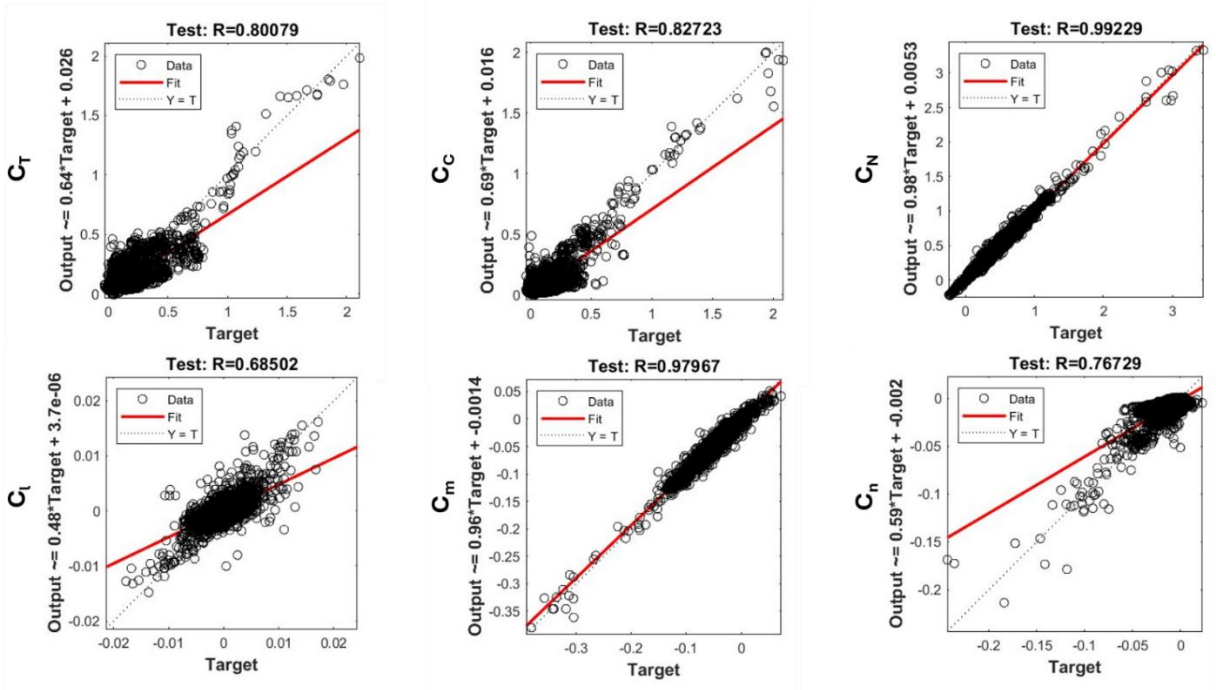


Figure 13 – Data regression for the Neural Network estimation method.

In Figure 14, a comparison of raw flight test data with the Linear and Neural Network methods is shown for a longitudinal excitation. The input in form of elevator (δ_e) and canard (δ_c) deflection from a trimmed state is used.

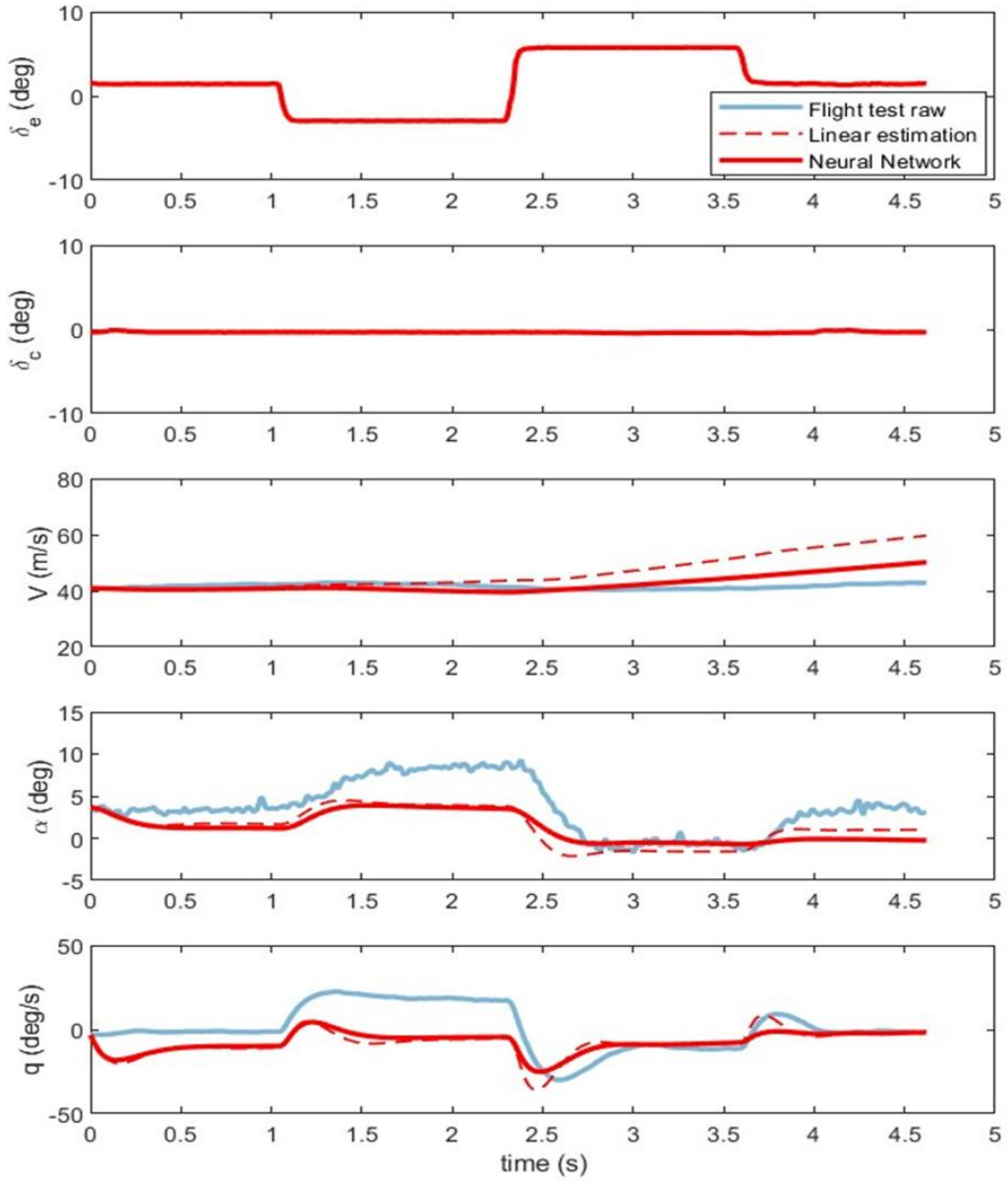


Figure 14 – Flight test vs. simulation.

4. Discussion

As can be seen in the results in Figure 12, both the Linear and the Neural Network identification methods perform fairly well within the envelope where flight test data is present. Outside this envelope, care should be taken since the characteristics might not be linear and also the Neural Network function is very flexible and therefore relies heavily on the data used. The exception from the performance of the methods is the estimation of the tangential force coefficient (C_T). This coefficient is in general hard to estimate, but here this could also be an effect of the engine data. The accuracy of the measurement for the engine thrust cannot be guaranteed.

The estimations of the normal force (C_N) and pitching moment (C_m) coefficients seem to be the most accurate, following the raw flight test data. This can also be seen in Figure 13, where the R-value is close to one. For the other coefficients the R-values are lower. One possible reason for this could be the limited excitation of control surface deflections and another could be the accuracy in sensor data and sensor position.

The nonlinearity of the Neural Network estimation for angle-of-attack above $20°$ look similar to that of the CFD and wind tunnel test data. This gives confidence that the Neural Network method can resolve this kind of nonlinear behavior in data. A separate estimation using the Linear method would have to be done between angle of attack $20°$ and $25°$ to catch this. This has not been done here.

Figure 14 shows a simulation using input data from a flight test excitation not used in the estimation of the model parameters. As can be seen there are some differences in the details, but also similarities in the trends. It looks like there is differences in the trim state since both the angle-of-attack and pitch rotation velocity change during the first second even though the input is unchanged. This is something that has to be investigated further. It should also be noted that the two identification methods perform similar for this simulation. This is not surprising since the excitation is performed in an envelope that most probably is linear in its characteristics.

In this paper, only flight test data has been used for the identification of the aerodynamic model. However, it would also be possible to use flight test data together with data from other sources, like wind tunnel tests and CFD calculations to catch nonlinearities better and to span a larger flight envelope for coming flights. This could possibly increase the accuracy of the estimations. This will be investigated in the future.

5. Conclusion

Using Neural Network functions for system identification is possible. It can handle nonlinear system behavior. Since the method relies heavily on data available, as much data as possible should be used to cover the envelope of interest. More work is needed to improve the accuracy when looking into simulating flight test data.

6. Contact Author Email Address

mailto: roger.gunnar.larsson@saabgroup.com.

7. Copyright Statement

The authors confirm that they, and/or their company or organization, hold copyright on all of the original material included in this paper. The authors also confirm that they have obtained permission, from the copyright holder of any third party material included in this paper, to publish it as part of their paper. The authors confirm that they give permission, or have obtained permission from the copyright holder of this paper, for the publication and distribution of this paper as part of the ICAS proceedings or as individual off-prints from the proceedings.

References

[1] Jouannet C, et. al. Subscale flight testing used in conceptual design. Aircraft Engineering and Aerospace Technology, Vol. 84, No. 3, pp 192-199, 2012.

[2] Lundström D. *Aircraft Design Automation and Subscale Testing, with Special Reference to Micro Air Vehicles.*, Linkopings Universitet (Sweden), 2012.

[3] Sobrón A. *On Subscale Flight Testing Cost-Effective Techniques for Research and Development*., Linkopings Universitet (Sweden), 2021.

[4] Ljung L. *System identification-theory for the user*. 2nd edition, Prentice-hall, 1999.

[5] Bishop C M. *Pattern recognition and machine learning*., Springer google schola 2, pp1122-1128., 2006

[6] Morelli, E A. "Practical aspects of real-time modeling for the learn-to-fly concept." 2018 Atmospheric Flight Mechanics Conference. 2018.

[7] Morelli, E A. "Global nonlinear parametric modelling with application to F-16 aerodynamics." Proceedings of the 1998 American Control Conference. ACC (IEEE Cat. No. 98CH36207). Vol. 2. IEEE, 1998.